Korean J. Chem. Eng., **26**(5), 1405-1413 (2009)
DOI: 10.1007/s11814-009-0220-9

CFD simulation of gas-solid bubbling fluidized bed containing FCC particles

Seyyed Hossein Hosseini†, Rahbar Rahimi, Mortaza Zivdar, and Abdolreza Samimi

Department of Chemical Engineering, University of Sistan and Baluchestan, Zahedan 98164-161, Iran
(*Received 26 January 2009 • accepted 5 March 2009*)

Abstract−The hydrodynamics of a bubbling gas-solid fluidized bed of 57.4 μm FCC particles was simulated by using a state-of-the-art two-fluid model integrating the kinetic theory of granular flow for particulate phase stresses. The overestimation of the bed expansion was resolved by using a suitable scale factor in the drag model as suggested by McKeen and Pugsley (T.R. McKeen, T.S. Pugsley, Powder Technol., 129, 139 (2003)). This study showed that the method was appropriate in simulation of a gas-solid fluidized bed of Geldart A particles at high gas velocities (0.3 to 0.61 m/s). The reduction of computational time especially for simulation of large-scale systems was achieved. The time-averaged local voidage was compared with the experimental data and the trend of varying several parameters on the hydrodynamic of the bed was investigated. The simulation results showed both qualitative and quantitative agreement with the literature.

Key words: Bubbling Fluidized Bed, FCC, CFD

INTRODUCTION

Fluidization systems are applied extensively in a variety of industries such as those involving fluid catalytic cracking units. Their favorable characteristics are high heat and mass transfer rates and their continuous particle handling ability. Since the performance of a fluidized bed greatly depends on the hydrodynamics of the system, its modeling and simulation are essential. It is a challenging problem as the complexity of flow behavior is high and many interactions are involved. Of the various modeling and simulation techniques, computational fluid dynamics (CFD) is employed in this article. CFD has been used as a powerful numerical tool for modeling of multiphase flows and reduction of the design time and cost [1-5]. CFD is divided into the Lagrangian and Eulerian approaches, which are compared in the literature [6-8]. The Lagrangian approach describes the solid and the gas phases at particle level and as a continuum, respectively. In the Eulerian method, the two involved phases (gas and solid) are treated as fully interpenetrating continua. Owing to the assumption of continuum behavior of the solid phase, the particulate phase requires additional closure laws to describe the rheology of the fluidized particles reasonably. The kinetic theory of granular flow was employed for this purpose. Kinetic theory based on granular temperature (Θ_s) is ideally suited to describe elastic random oscillations of particles suspended in the fluid [9,10].

Several Eulerian-Eulerian simulations of a bubbling fluidized bed (BFB) of Geldart group B and D particles have been reported in the literature with a fair degree of success and varying degrees of model validation [11-15], but few successful cases for modeling Geldart A systems have been reported due to the complexity of handling the effect of interparticle forces.

Cohesive interparticle forces have been reported to be significant for fine Geldart A and C particles [16,17]. It is extremely difficult to measure the cohesive forces between Geldart A particles directly, since this type of force strongly depends on the surface properties of particles. This is so even though the clustering phenomenon in fluidized beds with Geldart A particles is the result of the effect of interparticle forces and particle-particle collisions which are not well known. Therefore, more investigation on this effect using Geldart A particles is required.

Several authors observed overestimation of bed expansion by using an Eulerian-Eulerian approach in simulation of BFB containing Geldart A particles [18-20]. Bayle et al. [19] speculated that the drag laws and solids viscosity relations in their model need improvement for solving over-predicted bed expansion. Krishna and van Baten [21] proposed a new limited model of pseudo-fluids. In their model, properties of emulsion phase were set as constant and empirical correlations of mean bubble diameter and rise velocity were used. Another attempt was made by Kim and Arastoopour [22,23] to modify the kinetic theory of granular flow. They introduced a very complex cohesive force model. But, their model is limited in use, due to requirements of empirical inputs such as particle surface energy, which are not well defined. McKeen and Pugsley [24] simulated a freely bubbling bed of fluid catalytic cracking (FCC) catalyst for a superficial gas velocity in low range of 0.05-0.2 m/s. They argued that their modification was attributed to the formation of clusters with a size smaller than the CFD grid size, leading to an overall smaller drag force acting in the particle bed. Zimmermann and Taghipour [25], by using the modified drag law of Syamlal and O'Brien [26], have simulated the BFB of FCC particles and reported that the bed expansion and radial void fraction are in a good agreement with the experimental data. This method has limited range of applicability [27]. Mao Ye et al. [28,29] simulated the fluidized bed of Geldart A particles at low gas velocity by two methods, modification of the standard drag law of Wen-Yu and solid properties depending on granular temperature; their procedure is limited to low range of gas velocity.

Recently Wang et al. [30] for the first time have been shown that two-fluid model (TFM) can predict the correct bed expansion at gas velocity range 0.006-0.018 m/s, without any artificial modifications using sufficiently fine grid size and small time step. Their method is not appropriate for a large-scale fluidized bed, and should be

†To whom correspondence should be addressed.
E-mail: hosseini@mail.usb.ac.ir

tested for high gas velocities.

In respect to the above considerations, the objective of the current study was to model the hydrodynamics of a bubbling FCC fluidized-bed by using the modified standard drag model at high gas velocities. The results of simulations were compared with the available experimental data. Also, the local trends of a number of hydrodynamic parameters were investigated.

NUMERICAL METHOD

1. Hydrodynamic Model

Simulation of a fluidized bed using the Eulerian-Eulerian approach requires a set of momentum and continuity equations for each phase. These equations were linked through pressure and interphase exchange relationships as given by Eqs. (2) to (4) in Table 1. External body, lift and virtual mass forces are assumed negligible in the momentum equations. The granular temperature, Θ_s Eq. (5) in Table 1 describes conservation of the kinetic energy for particulate phase.

The drag model of Gibilaro et al. [31] was chosen because it is a single, simple, compact and continuous function over all values of void fraction. The dense solid phase containing inelastic spherical particles was modeled based on the kinetic theory of granular flow (KTGF). The equation of Lun et al. [32] was used for solid granular bulk viscosity. The expression of Schaeffer [32] was used for fric-

Table 1. Governing equations for two-fluid model

Continuity equation for qth phase without any mass transfer between the phases

$$\frac{\partial}{\partial t}(\alpha_q\rho_q)+\nabla\cdot(\alpha_q\rho_q\vec{v}_q)=0,\ \ \sum\alpha_q=1 \tag{2}$$

Conservation of momentum equations for gas phase

$$\frac{\partial}{\partial t}(\alpha_g\rho_g\vec{v}_g)+\nabla\cdot(\alpha_g\rho_g\vec{v}_g\vec{v}_g)=-\alpha_g\nabla P+\nabla\cdot\bar{\bar{\tau}}_g+\alpha_g\rho_g g-K_{gs}(\vec{v}_g-\vec{v}_s) \tag{3}$$

Conservation of momentum for solid phase

$$\frac{\partial}{\partial t}(\alpha_s\rho_s\vec{v}_s)+\nabla\cdot(\alpha_s\rho_s\vec{v}_s\vec{v}_s)=-\alpha_s\nabla P-\nabla P_s+\nabla\cdot\bar{\bar{\tau}}_g+\alpha_s\rho_s g+K_{gs}(\vec{v}_g-\vec{v}_s) \tag{4}$$

Fluctuating energy equation for particles $\left(\Theta=\frac{1}{3}\langle v_s'^2\rangle\right)$

$$\frac{3}{2}\left[\frac{\partial}{\partial t}(\alpha_s\rho_s\Theta_s)+\nabla\cdot(\alpha_s\rho_s\vec{v}_s\Theta_s)\right]=(-P_s\bar{\bar{I}}+\bar{\bar{\tau}}_s):\nabla\vec{v}_s+\nabla\cdot(k_{\Theta s}\nabla\Theta_s)-\gamma_{\Theta s}+\phi_{gs} \tag{5}$$

Table 2. Closure relationships for two-fluid model

Stress-strain tensor for qth phase

$$\bar{\bar{\tau}}_s=\alpha_q\mu_q(\nabla\vec{v}_q+\nabla\vec{v}_q^T)+\alpha_q\left(\lambda_q-\frac{2}{3}\mu_q\right)\nabla\cdot\vec{v}_q\bar{\bar{I}} \tag{6}$$

Radial distribution function

$$g_{0,ss}=\frac{1+2.5\alpha_s+4.5904\alpha_s^2+4.515439\alpha_s^3}{\left[1-\left(\frac{\alpha_s}{\alpha_{s,max}}\right)\right]^{3-0.67802}} \tag{7}$$

Collision dissipation energy

$$\gamma_{\Theta m}=\frac{12(1-e_s^2)g_{0,ss}}{d_s\sqrt{\pi}}\rho_s\alpha_s^2\Theta_s^{3/2} \tag{8}$$

Transfer of kinetic energy

$$\phi_{gs}=-3K_{gs}\Theta_s \tag{9}$$

Solid pressure

$$P_s=\alpha_s\rho_s\Theta_s+2\rho_s(1+e_s)\alpha_s^2g_{0,ss}\Theta_s \tag{10}$$

Solid shear viscosity

$$\mu_s=\frac{4}{5}\alpha_s\rho_sd_sg_{0,ss}(1+e_s)\left(\frac{\Theta_s}{\pi}\right)^{1/2}+\frac{10d_s\rho_s\sqrt{\Theta_s\pi}}{96(1+e_{ss})g_{0,ss}}\left[1+\frac{4}{5}\alpha_sg_{0,ss}(1+e_s)\right]^2+\frac{P_s\sin\phi}{2\sqrt{I_{2D}}} \tag{11}$$

Solids Thermal Conductivity

$$k_{\Theta s}=\frac{150d_s\rho_s\sqrt{\Theta_s\pi}}{384(1+e_s)g_{0,ss}}\left[1+\frac{6}{5}\alpha_sg_{0,ss}(1+e_s)\right]^2+2\rho_sd_s\alpha_s^2g_{0,ss}(1+e_s)\sqrt{\frac{\Theta_s}{\pi}} \tag{12}$$

Drag model

$$K_{gs}=0.1\left(\frac{17.3}{Re_p}+0.336\right)\frac{\rho_g|\vec{v}_s-\vec{v}_g|}{d_p}\varepsilon_s\varepsilon_g^{-1.8}\ \text{where}\ Re_p=\frac{\rho_gd_p|\vec{v}_s-\vec{v}_g|\varepsilon_g}{\mu_g} \tag{13}$$

tional viscosity with an angle of internal friction of 30°. Using this term leads to better results in dense gas-solid fluidized bed [15,33-35].

Similar to several researchers, the restitution coefficient of 0.9 was used in the current simulation [24,25,36]. Both models of Gidaspow [32] and Syamlal et al. [32] for solid shear viscosity and solid thermal conductivity terms yield the same results at solid volume fraction higher than 0.2 [37,38]. Thus, solid shear viscosity and solid thermal conductivity of Gidaspow [32] were used. Researchers have shown that all radial distribution functions are eventuated to similar simulation results [37,38]. Based on previous studies for dense bubbling fluidized bed systems, the Ma and Ahmadi [40] radial distribution function was used in the current model [15,28-30,33,39]. Table 2 represents the constitutive equations, Eqs. (6) to (13), which were used in this simulation.

2. Simulation Setup

Lettieri and others [41,42] investigated the existence of consistency between 2D and 3D simulations. They recommend the use of 2D models for the reduction of computational time. The experimental data of Ellis [43] in a fluidized bed of 0.286 m diameter and 4.5 m height were used for validation of the model. It should be noted that the freeboard of the bed must be high enough to obtain fully developed flow. Considering this point and saving the computational time, actual computational domain of 0.286 m×1.6 m was simulated to make sure no solid particles exist in the upper region of the bed.

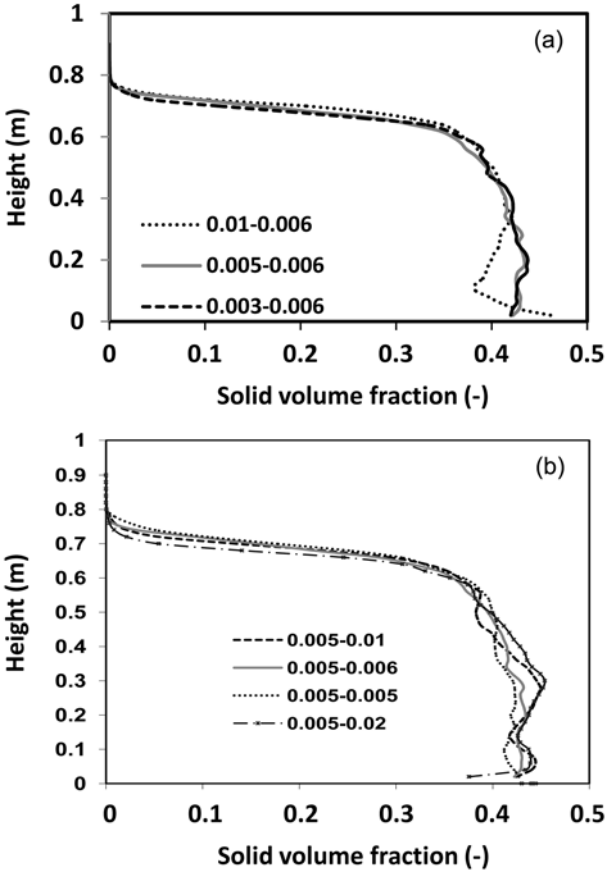

Fig. 1. Investigation of mesh-independency in both directions: (a) x-direction, (b) y-direction.

Table 3. Specifications of the fluidized bed

Property	Value
Superficial gas velocity (m/s)	0.3-0.61
Saunter mean diameter (μm)	57.4
Particle density (kg/m^3)	1560
Static bed height (m)	0.51
Voidage (-)	0.45

To obtain independency of the CFD results on the mesh size, simulations were carried out using different values of grid size in horizontal and vertical directions. For this reason, the time-averaged solid volume fraction along the bed was investigated as shown in Fig. 1. It can be seen that the grid number of 57 in horizontal direction with non-equal grid space and uniform grid size of 0.006 m in vertical direction are sufficiently fine for providing reasonable mesh independent results (case of 0.005-0.006). Near the wall the velocity gradients is high, so the used grids were denser than those away from the walls.

The governing equations in this system were solved by finite volume approach. First and second order upwind discretization schemes for volume fraction and momentum terms were used, respectively. The time steps of 0.00025 and 40 iterations per each time step were required to achieve full numerical convergence. A convergence criterion of 10^{-3} for each scaled residual component was fixed for the relative error between two iterations. The phase-coupled PC-SIMPLE algorithm was used for the pressure-velocity coupling. Table 3 summarizes the particle properties and operating condition of the bed.

3. Initial and Boundary Conditions

The gas velocities in the settled bed region and freeboard were set on $U_g/\alpha_{g,mf}$ and U_g, respectively. A very small solids volume fraction (~10^{-9}) was set for the particle phase in the freeboard because zero value of solid volume fraction at the upper section of bed can lead to unrealistic values of the particle and gas velocity field and poor convergence. At the initial solid static height of 0.51 m, the solid volume fraction was set 0.55. The left and right walls of the fluidized bed were treated as no slip boundary conditions for the both phases. The Dirichlet boundary conditions were employed at the bottom of the bed to specify a uniform gas inlet velocity and the pressure boundary conditions were set at atmospheric at the top of the freeboard.

RESULTS AND DISCUSSION

1. Investigation of Drag Model

The basic limitation of all gas-solid drag laws is that they are fitted with data for particles much larger than the fine Geldart A particles. Thus, the effect of interparticle forces leading to particle agglomeration and reducing drag force is not accounted for [24]. Gibilaro et al. [31] based on the Ergun equation [32] defined an improved dependency of voidage to better match both packed bed data and single particle drag. Li et al. [27] derived a continuous expression of the scale factor in the Gibilaro et al. [31] drag model for simulation of a horizontal jet fluidized bed.

Fig. 2 shows the quantitative comparison of different drag mod-

els at a constant slip velocity of 0.5 m/s and for the FCC particles used in the current study. As it is seen there is no significant difference between drag coefficients predicted by the models at all values of solid volume fraction.

Like the other simulations, in this work, avoiding the overestimation of bed expansion was impossible by using standard drag models. Fig. 3 shows the over-predicted bed expansion by using standard drag law of Wen and Yu [32]. To introduce the effect of particle agglomeration on the gas-solid drag force, a scale down of the Gibi-

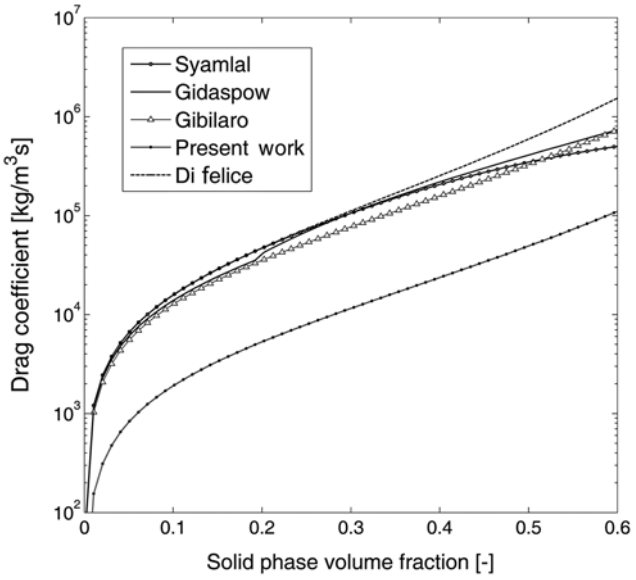

Fig. 2. Comparison of different drag models for FCC particles at the slip velocity of 0.5 m/s.

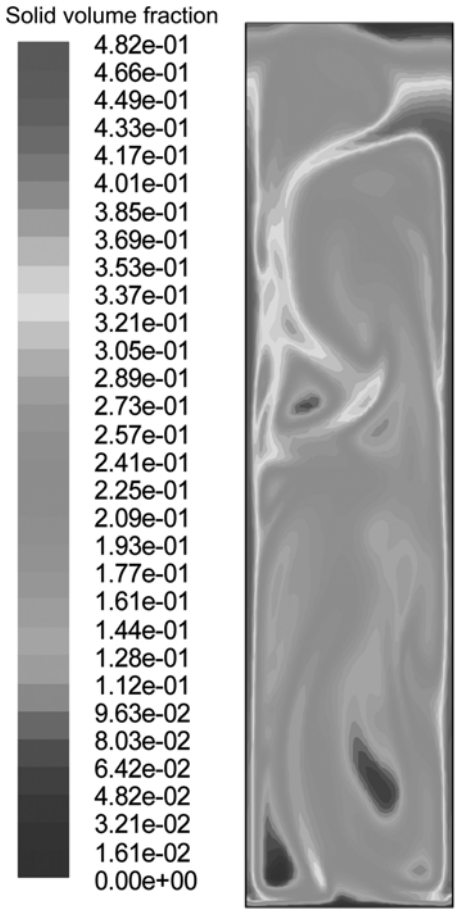

Fig. 3. Contour plot of solid volume fraction with standard drag model.

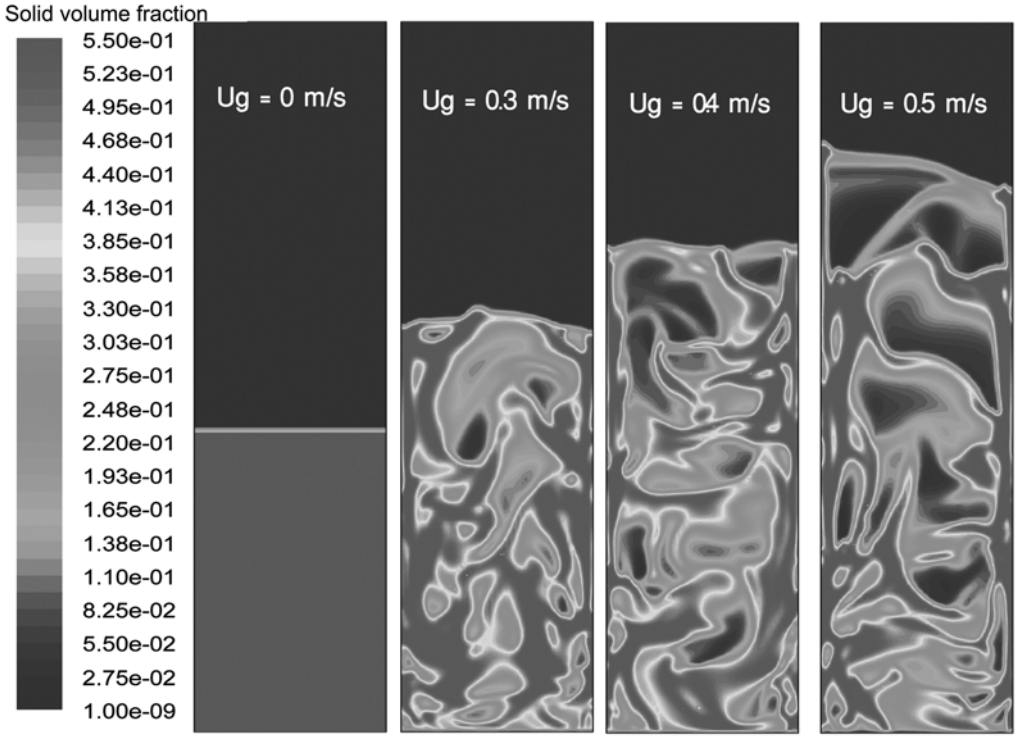

Fig. 4. Contour plot of solids volume fraction with different gas velocities.

laro et al. [31] drag model was used. The reduction of drag force by using a suitable scale factor is shown in Fig. 2. The value of scale factor (SF) should be less than one to reduce the drag force.

McKeen and Pugsley [24] obtained the SF of 0.25 for 75 μm particles at low value of gas velocity in their system. In this study, an SF of 0.1 was used as it was an appropriate value to obtain suitable bed expansion and local time-averaged voidage. By comparison of the present work and McKeen and Pugsley results, it is found that by decreasing the particle diameter, the SF must be decreased. This leads to more reduction in drag force, because with decreasing the particle diameter the cohesive force increases. The 27% bed expansion simulated in this work shows a good agreement with the 20% bed expansion obtained experimentally.

2. Qualitatve Comparisons

To investigate the suitable discretization schemes, it was found that by using the second order upwind for momentum term, the bubble size will be more realistic, and by using the QUICK scheme for the volume fraction term a clear bubble boundary as compared with first order upwind is obtained. In addition, the first order upwind leads to easier solution convergence as compared to second order upwind and QUICK schemes. This finding can be useful for other works associated with bubble properties.

As the fluidization proceeds, the bubbles split and coalesce continuously. Fig. 4 shows the contour plot of solid volume fraction for the superficial gas velocities of 0.3, 0.4 and 0.5 m/s. The bubble formation causes bed expansion. This figure shows that the bed expansion increases with the increase of superficial gas velocity. Furthermore, the higher gas velocity causes formation of larger bubbles. This issue also has been confirmed by researchers [25,44]. The experimental observations indicated small bubble formation near the distributor and large bubbles at the top of the bed as the bubbles coalesce and grow during their rise to the top of the bed [15,24,37, 42]. Large bubbles form in the middle of the bed because of more bubble coalescence in this region. The reasons would be due to the wall effects and interaction between the bubbles. Those behaviors are also shown in Fig. 4.

3. Local Voidage

After the first five seconds the quasi-steady-state was reached; therefore, the time averaged distributions of flow variables were computed after the steady state conditions, from 5 s to 25 s. Fig. 5 shows the voidage, gas volume fraction, at U_g=0.3 m/s at several bed heights. As it is seen, both experimental and simulation results are asymmetric with respect to the centerline of the bed; at 0.15 m above the distributor and higher axial level, more symmetrical behavior is observed. Fig. 5 also shows that the radial distribution of gas phase volume fraction is a strong function of height above the distributor. As shown, with increasing axial level of the bed (h), the gas volume fraction increases at all radial positions especially at the central region.

The influence of axial position on the radial profiles of voidage is displayed in Fig. 6 at different gas velocities (U_g=0.4, 0.5 and 0.6 m/s). At constant level of the bed with increasing the gas velocity, the voidage (gas volume fraction) increases. Also, for each gas velocity, the voidage increases with increasing the axial level of the bed.

Enhancing the voidage in the central region of the bed and a high volume fraction of particles near the wall as shown in Figs. 5 and 6 is due to the considerable passage of bubbles in the central area and recirculation of the particles near the wall. This behavior is in accord with the experimental observations [45]. Any discrepancy between the experimental and simulation results could be due to the effect of the gas distributor, which was not considered in simulations and using 2D instead of 3D modeling (cylindrical systems).

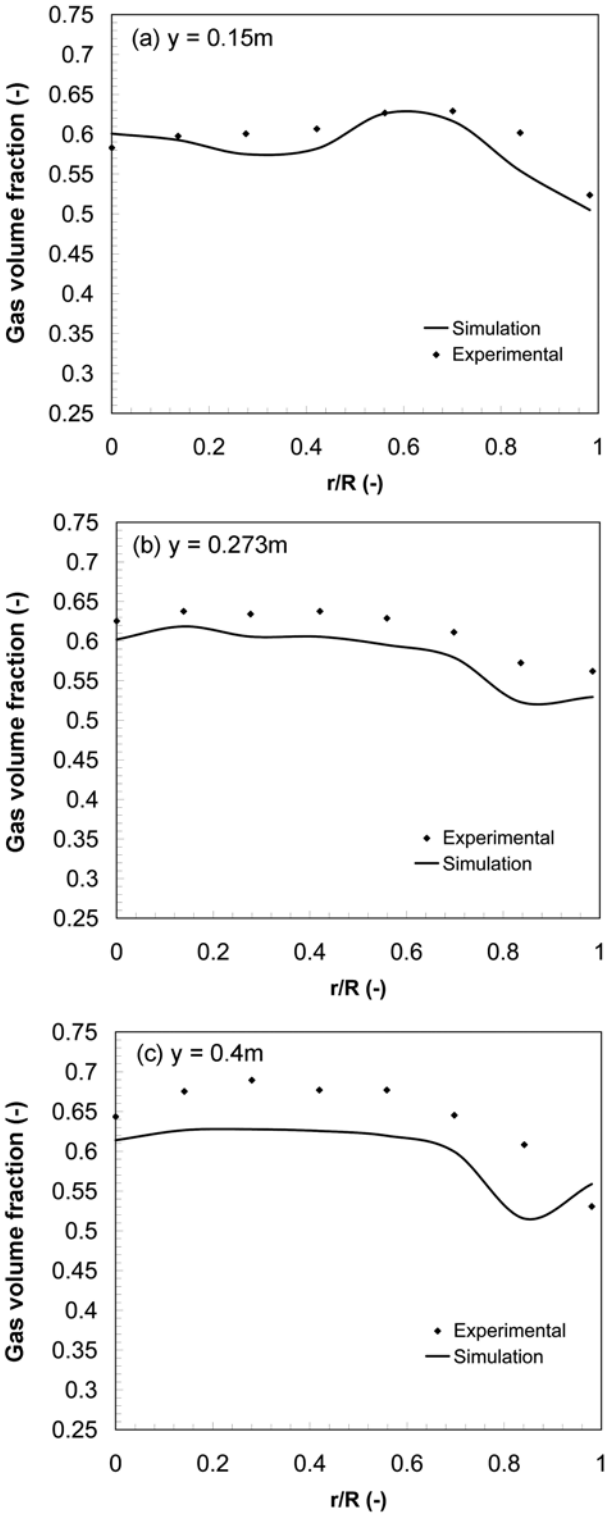

Fig. 5. Radial voidage distribution at U_g=0.3 m/s and various axial levels.

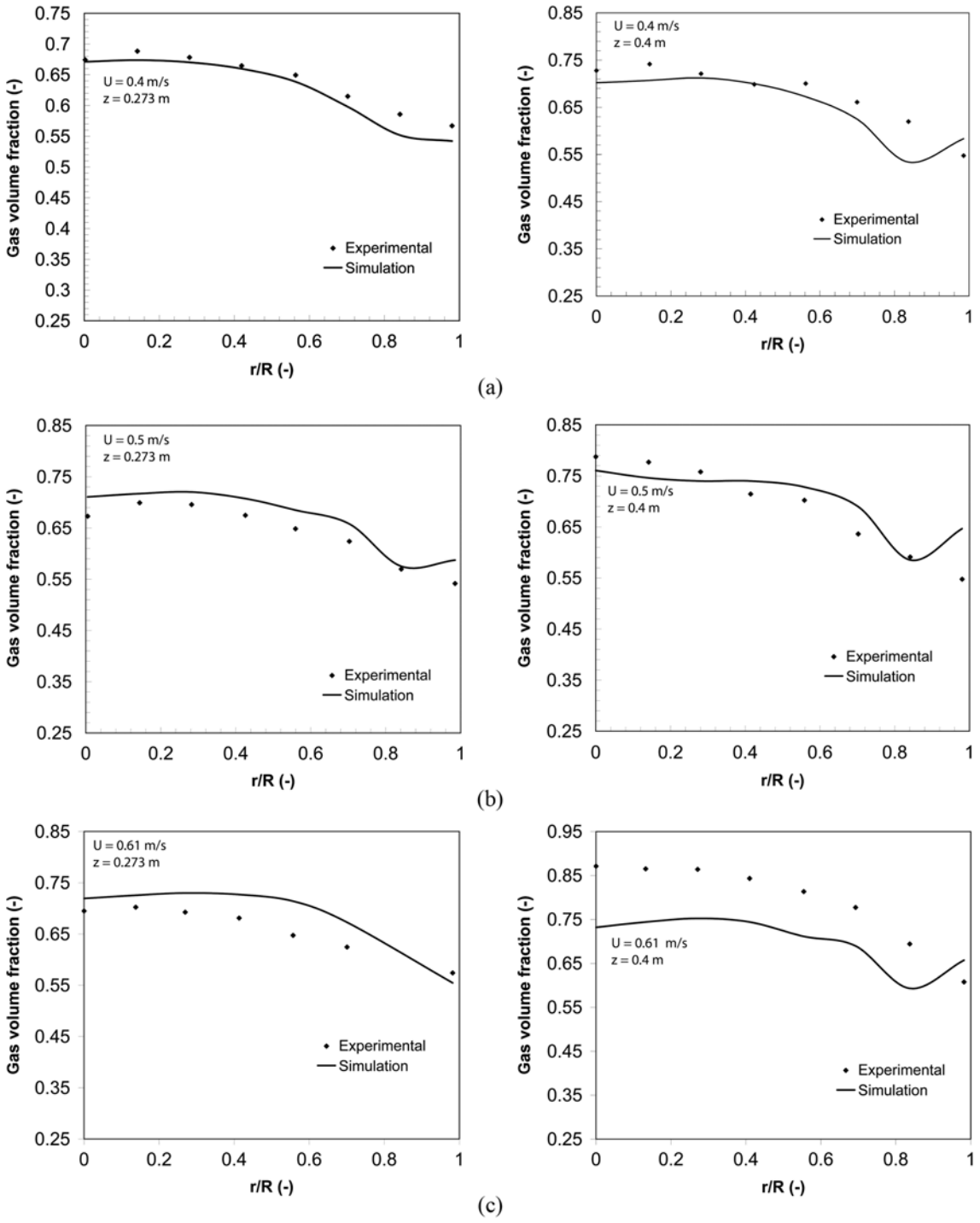

Fig. 6. Radial voidage distribution at various gas velocities, (a) 0.3, (b) 0.4, (c) 0.5 and (d) 0.6 m/s, and two axial levels of 0.273 and 0.4 m.

Table 4. RMS at different gas velocities

Gas velocity, m/s	0.3	0.4	0.5	0.61
RMS (at y=0.15 m)	4.17	-	-	-
RMS (at y=0.273 m)	5.39	2.95	5.08	5.86
RMS (at y=0.4 m)	8.62	6.28	7.56	12.83

Root mean square-deviation (RMS) criteria at different velocities (0.3, 0.4, 0.5 and 0.6 m/s) are presented in Table 4 and computed as:

$$\delta_{RMSD} = \left[\frac{1}{N}\sum_{1}^{N}\left(\frac{X_{Experimental} - X_{Computational}}{X_{Experimental}}\right)^2\right]^{1/2} \times 100 \quad (1)$$

The method presented here shows a better agreement with the experimental data and needs a lower number of cells compared to the other methods such as modified drag model of Syamlal-O'Brien [25]. Therefore, this method can be considered for simulation of industrial fluidization systems.

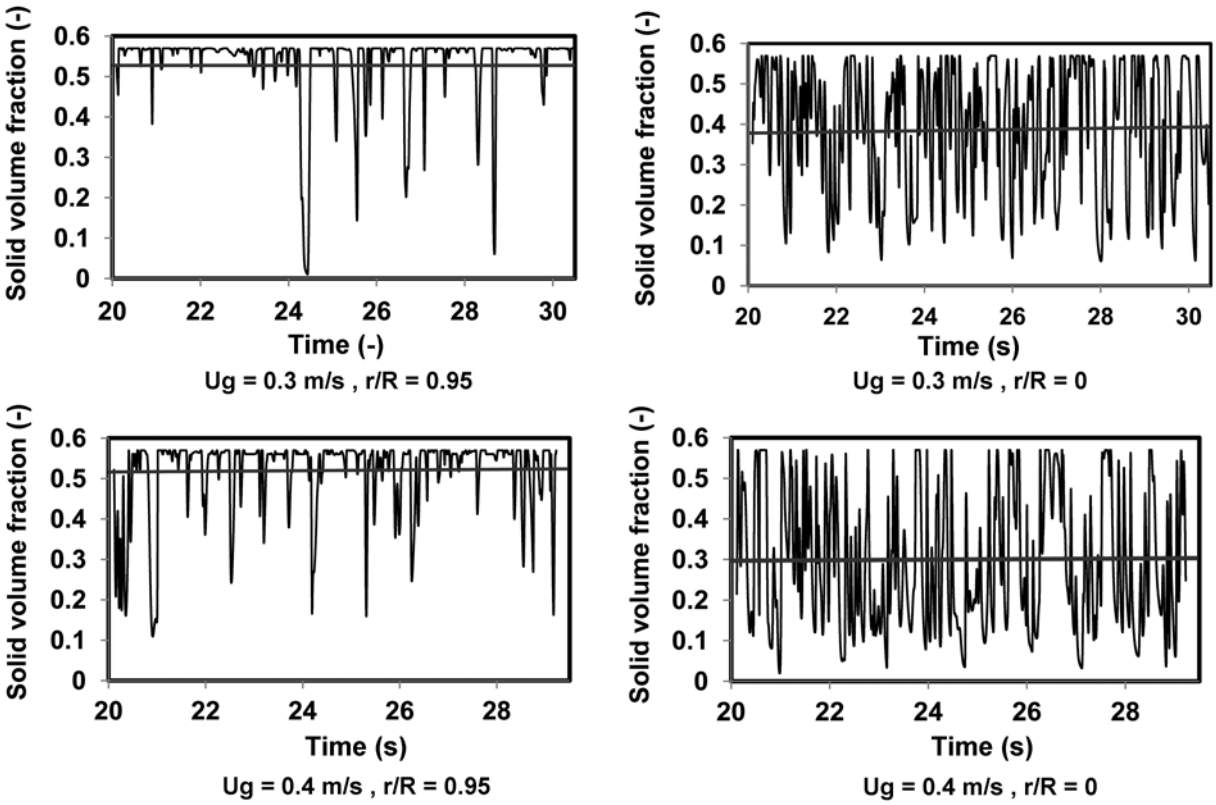

Fig. 7. Instantaneous solid concentration at various U_g and different radial position.

4. Instantaneous Solid Concentration

Analysis of the temporal behavior of the local solid concentration can provide much useful information for the hydrodynamics of a fluidized bed. It can lead to a greater understanding of the flow pattern of these systems.

Fig. 7 shows the instantaneous local solids concentration at different radial positions (r/R=0 and 0.95) at U_g=0.3 and 0.4 m/s at z=0.5 m. In this figure, the solid horizontal lines show the average solid concentration. With increasing U_g, the solid concentration fluctuations become more intensive at both radial positions due to increasing the interactions between two phases. In addition, the magnitude and intensity of the fluctuations at the two positions are different. With increasing the gas velocity, the average solid concentration decreases at both positions, especially at the central area. However, the fluctuations of solid concentration at the central region of the bed are stronger than the wall region. Furthermore, with moving toward the wall, there is an obvious decrease in the bubble frequency and the solids content in the bubbles becomes higher as compared to the central region. This is in line with the experimental result of Zhu et al. [46]. By considering the validated model qualitatively and quantitatively, the current model can be used as a suitable predictor tool to obtain detailed information of the hydrodynamics parameters of the bed.

5. Particles Velocity

One of the important parameters in the flow pattern of a fluidized bed is the particle velocity. By obtaining a suitable solid velocity profile, several phenomena such as heat and mass transfer can certainly be investigated. Fig. 8 shows the results of CFD simulation of time-averaged particle velocities for gas velocity of 0.3 m/s at

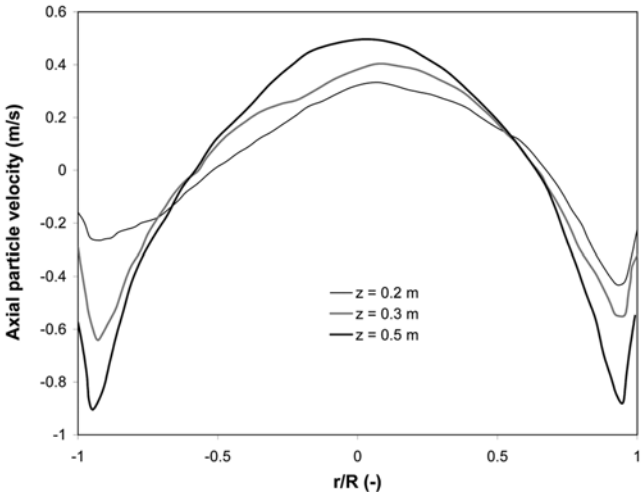

Fig. 8. Time-averaged radial distribution of particles velocity at different axial level (U_g=0.3 m/s).

three beds' axial locations, z, equal to 0.2, 0.3 and 0.5 m. As can be seen, particles are rising in the center of the bed and falling down close to the wall. Fig. 9 shows the time-averaged axial particle velocity at U=0.3 m/s versus height above the distributor in the center of the bed, which is a further explanation of solid hydrodynamics. As shown in Fig. 9 at z equals to 0.46 m, the time-averaged axial solid velocity is at its highest value of 0.5 m/s. An experimental validation of this phenomenon, which is vital in heat and mass transfer studies, is required. From Figs. 8 and 9 it can be found that by in-

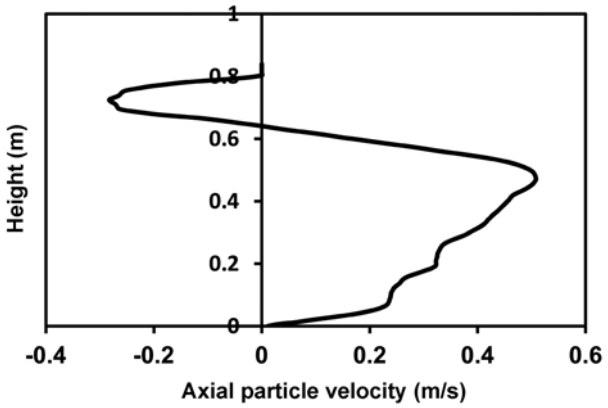

Fig. 9. Time-average axial solid particles at central line of the bed (U_g=0.3 m/s).

creasing the axial location, the axial particle velocity is increased to its maximum then reduced with further increasing of z. As can be seen from Fig. 8, downfall of particles near the wall shows similar trend, i.e., at a constant level of the bed, with increasing the upward particle velocity in the center of the bed, downward particle velocity increases also.

CONCLUSIONS AND FUTURE WORK

A state-of-the-art two-fluid model integrating kinetic theory for emulsion phase has been used to investigate unsteady state behavior of a bubbling FCC fluidized-bed at high gas velocities. The model was found to be suitable for simulation of BFB containing Geldart A particles. The cohesive forces are accounted for by lowering the SF of Gibilaro et al. [31] drag model. CFD results show that the method suggested by McKeen and Pugsley [24] can be used at high gas velocities. This model indicates the suitable trend of several hydrodynamic parameters that are confirmed by researchers [24,25, 37,44-46]. Some aspects of hydrodynamic behavior of the particle flow pattern were predicted that they need more experimentation. Consequently, the current method can be used at different scale of the fluidized beds. This includes various FCC particle diameters and different range of gas velocities. Confirmation awaits experimental data of industrial scale fluidized bed. More investigation to derive a general SF applicable to different conditions is required.

ACKNOWLEDGMENT

The authors gratefully acknowledge the comments and guidance of Dr. Junwu Wang at Twente University.

NOMENCLATURE

C_D : drag coefficient [-]
d_i : diameter [m]
e_s : restitution coefficient [-]
e_w : wall restitution coefficient [-]
g : acceleration due to gravity [m/s^2]
$g_{0,ss}$: radial distribution coefficient [-]
h : height above the distributor [-]
$\bar{\bar{I}}$: stress tensor [-]
I_{2D} : second invariant of the deviatoric stress tensor [-]
$k_{\Theta s}$: diffusion coefficient for granular energy [kg/m s]
K_{gs} : gas/solid momentum exchange coefficient [kg/m^3 s]
P : pressure [-]
r : radial coordinate [-]
R : radius [-]
Re_p : Reynolds number [-]
t : time [-]
U_g : superficial gas velocity [m/s]
v_i : velocity [m/s]
z : height coordinate measured from distributor [m]
v_s' : fluctuating particle velocity of the particulate phase [m/s]

Greek Letters

α_i : volume fraction [-]
$\gamma_{\Theta s}$: the collisional dissipation of energy [kg/s^3 m]
Θ_s : granular temperature [m^2/s^2]
λ_i : bulk viscosity [kg/m s]
μ_i : shear viscosity [kg/m s]
ρ_i : density [kg/m^3]
$\bar{\bar{\tau}}_i$: stress tensor [Pa]
ϕ : angle of internal friction [deg]
ϕ_{gs} : transfer rate of kinetic energy [kg/s^3 m]

Subscripts

col : collision
fr : friction
g : gas
i : general index
kin : kinetic
mf : minimum fluidization
p : particle
q : phase type (solid or gas)
s : solids
T : stress tensor

REFERENCES

1. J. Kim and G. Y. Han, *Korean J. Chem. Eng.*, **24**, 445 (2007).
2. B. Chalermsinsuwan, P. Kuchonthara and P. Piumsomboon, *Chem. Eng. Process.*, **48**, 165 (2009).
3. W. Zhong, Y. Zhang, B. Jin and M. Zhang, *Chem. Eng. Technol.*, **32**(3), 1 (2009).
4. V. A. Danilov, J. Lim, I. Moon and K. H. Choi, *Korean J. Chem. Eng.*, **23**, 753 (2006).
5. Y. Park, C. Y. Yun, J. Yi and H. Kim, *Korean J. Chem. Eng.*, **22**, 697 (2005).
6. V. V. Ranade, *Computational flow modeling for chemical reactor engineering*, 1st, ed., Academic Press (2002).
7. M. Chiesa, V. Mathiesen, J. A. Melheim and B. Halvorsen, *Comput. Chem. Eng.*, **29**, 291 (2005).
8. M. A. van der Hoef, M. van Sint Annaland and J. A. M. Kuipers, *Chem. Eng. Sci.*, **59**, 5157 (2004).
9. J. T. Jenkins and S. B. Savage, *J. Fluid Mech.*, **30**, 187 (1983).
10. C. K. K. Lun, S. B. Savage, D. J. Jeffrey and N. Chepurniy, *J. Fluid Mech.*, **140**, 223 (1984).

11. B. G. M. van Wachem, J. C. Schouten, R. Krishna and C. M. van den Bleek, *Chem. Eng. Sci.*, **54**, 2141 (1999).
12. J. Ding and D. Gidaspow, *AIChE J.*, **36**, 523 (1990).
13. C. C. Pain, S. Mansoorzadeh, C. R. E. de Oliveira and A. J. H. Goddard, *Int. J. Multiph. Flow*, **36**, 91 (2001).
14. B. G. M. van Wachem, J. C. Schouter, R. Krishna and C. M. van den Bleek, *Comput. Chem. Eng.*, **22**, S299 (1998).
15. D. J. Patil, M. van Sint Annaland and J. A. M. Kuipers, *Chem. Eng. Sci.*, **60**, 73 (2005).
16. L. Massimilla and G. Donsi, *Powder Technol.*, **15**, 253 (1976).
17. J. R. Grace and G. Sun, *Can. J. Chem. Eng.*, **69**, 1126 (1991).
18. G. Ferschneider and P. Mege, *Rev. Inst. Fr. Pet.*, **51**(2), 301 (1996).
19. J. Bayle, P. Mege and T. Gauthier, In: M. Kwauk, J. Li and W. C. Yang (Eds.), Fluidization X, Engineering Foundation, New York, p. 125 (2001).
20. T. Patureaux and D. Barthod, *Oil Gas Sci. Technol.-Rev. IFP*, **55**(2), 219 (2000).
21. R. Krishna and J. M. van Baten, *Chem. Eng. J.*, **82**, 247 (2001).
22. H. S. Kim and H. Arastoopour, *Can. J. Chem. Eng.*, **73**, 603 (1995).
23. H. S. Kim and H. Arastoopour, *Powder Technol.*, **122**, 83 (2002).
24. T. R. McKeen and T. S. Pugsley, *Powder Technol.*, **129**, 139 (2003).
25. S. Zimmermann and F. Taghipour, *Ind. Eng. Chem. Res.*, **44**, 9818 (2005).
26. M. Syamlal and T. J. O'Brien, *Office of fossil energy, national energy technology laboratory*, Morgantown, WV, April (1987).
27. T. Li, K. Pougatch, M. Salcudean and D. Grecov, *Powder Technol.*, **184**, 89 (2008).
28. M. Ye, J. Wang, M. A. van der Hoef and J. A. M. Kuipers, *Particuology*, **6**, 540 (2008).
29. M. Ye, Ph.D. Thesis, University of Twente, Enschede, Netherlands (2005).
30. J. Wang, M. A. vander Hoef and J. A. M. Kuipers, *Chem. Eng. Sci.*, **64**, 622 (2009).
31. L. G. Gibilaro, R. Di Felice and S. P. Waldram, *Chem. Eng. Sci.*, **40**(10), 1817 (1985).
32. Fluent 6.3, User's Guide, 23.5 Eulerian Model, Fluent Inc., (2006).
33. D. J. Patil, M. van Sint Annaland and J. A. M. Kuipers, *Chem. Eng. Sci.*, **60**, 57 (2005).
34. L. Huilin, H. Yurong, L. Wentie, D. Jianmin, D. Gidaspow and J. Bouillard, *Chem. Eng. Sci.*, **59**(4), 865 (2004).
35. W. Du, X. J. Bao, J. Xu and W. S. Wei, *Chem. Eng. Sci.*, **61**(14), 4558 (2006).
36. F. Taghipour, N. Ellis and C. Wong, *Chem. Eng. Sci.*, **60**, 6857 (2005).
37. B. G. M. van Wachem, J. C. Schouten, C. M. Bleek van den, R. Krishna and L. L. Sinclair, *AIChE J.*, **47**, 1035 (2001).
38. G. N. Ahuja and A. W. Patwardhan, DOI:10.1016/j.cej.2008.03.011.
39. D. J. Patil, J. Smit, M. van Sint Annaland and J. A. M. Kuipers, *AIChE J.*, **52**(1), 58 (2007).
40. D. Ma and G. Ahmadi, *J. Chem. Phys.*, **84**, 3449 (1986).
41. P. Lettieri, G. Micale, L. Cammarata and D. Colman, in Proc. 10th Workshop on Two-Phase Flow Predictions, Merseburg, 300 (2002).
42. L. Cammarata, P. Lettieri, G. D. M. Micale and D. Colman, *Int. J. Chem. Reactor Eng.*, **1**, A3 (2003).
43. N. Ellis, Ph.D. Thesis, University of British Columbia, Vancouver, British Columbia, Canada (2003).
44. Z. Yongmin and L. Chunxi, 3rd Asian Particle Technol. Symp., 392 (2007).
45. C. C. Pain, S. Mansoorzadeh and C. R. E. de Oliveira, *Int. J. Multiphase Flow*, **27**, 527 (2001**)**.
46. H. Zhu, J. Zhu, G. Li and F. Li, *Powder Technol.*, **180**, 339 (2008).